Journal of Nanostructure in Chemistry (2018) 8:153–158
https://doi.org/10.1007/s40097-018-0260-y

ORIGINAL RESEARCH

Low-temperature synthesis of core/shell of Co_3O_4@ZnO nanoparticle characterization and dielectric properties

Asma M. AlTurki[1]

Received: 4 February 2018 / Accepted: 19 March 2018 / Published online: 24 March 2018

Abstract

Cobalt oxide/zinc oxide core/shell nanoparticles (CZ NPs) were synthesized at low temperature by the sol–gel method. X-ray diffraction (XRD) was used for the detection of crystalline phases. Energy-dispersive analysis X-ray (EDAX) results for the sample as prepared showed that where only Co, Zn, C, and O was found, in forming CZ core/shell NPs. Transmission electron microscopy images indicated that the particles size of core/shell sample CZ NPs and the particles size were around 12 nm. The optical properties study by UV–Vis spectroscopy to estimate the bandgap of core/shell NPs. Frequency dependence dielectric was observed in core/shell NPs were prepared using the sol–gel method. Dielectric constant ε' and dielectric loss ε'' for CZ NPs were found to decrease with increasing frequency.

Graphical abstract

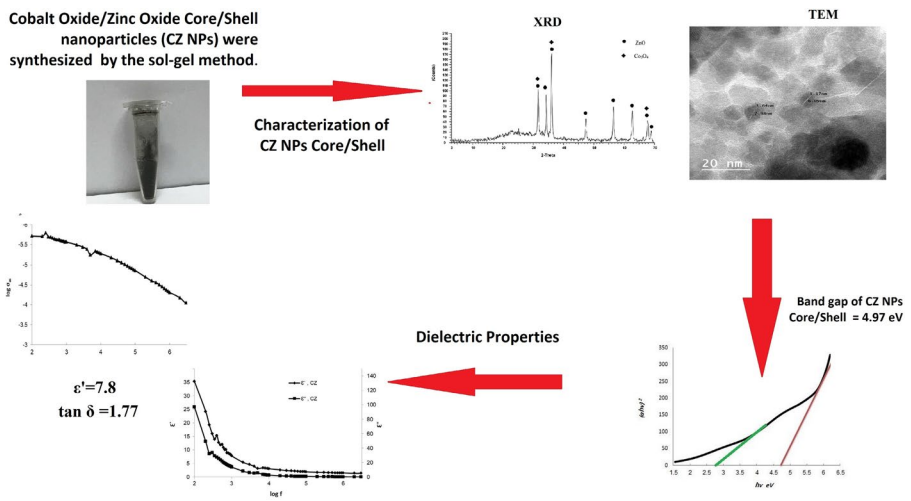

Keywords Cobalt oxide · Zinc oxide · Nanoparticles · Dielectric properties · Core/shell

Introduction

To purvey novel functionalities and properties massive efforts have been made to fabricate metal-based composites as metal/metal or metal oxide composites [1]. Core/shell nanoparticles (NPs) are a particular type of nanostructured material and its properties depend on the core–shell volume ratio [2, 3]. Core/shell nanoparticles are one of the solutions

✉ Asma M. AlTurki
aalturky@ut.edu.sa

[1] Department of Chemistry, Faculty of Science, University of Tabuk, Tabuk, Saudi Arabia

to obstacles in which an amendment in properties cannot be accomplished using one type of nanoparticles [4]. Employing a magnetic core can guide particles using an outer magnetic field. If a core/shell composite contains a magnetic core and semiconductor shell, the transmission and purging of the particles becomes potential [5]. Cobalt oxide Co_3O_4 magnetic nanoparticles are interesting due to its numerous oxidation states [6]. Zinc oxide (ZnO) semiconductor nanoparticles are on the forefront of research due to their special properties and massive usage [7]. ZnO-based materials are used in different applications, due to the photocatalytic nature, environmental sustainability, and low cost [8].

In the present work, we synthesized Co_3O_4/ZnO core/shell NPs using the sol–gel method. Structure, morphology, optical properties, dielectric, and magnetization were studied using EDAX, XRD, UV–Vis, TEM, and dielectric properties, respectively.

Materials and methods

Ammonium hydroxide Solution, Cobalt (II) Chloride purum p.a., anhydrous, ≥ 98%, Zinc chloride 97.6% obtained from Holyland (Saudi Arabia), Ethanol absolute was purchased from Sigma Aldrich Co. Ltd (USA). Acetic acid, glacial biochemical grade 99.86% purchased from ACROS.

Synthesis of ZnO (NPs)

For ZnO (NPs) prepared by a sol–gel method, we dissolved (1.35 g) of $ZnCl_2$ in a mixture of 20 mL of water and 5 mL NH_4OH and then added 80 mL of ethanol using a dropper for 60 min at 60 ºC while stirring for 2 h. The precipitate was filtered and washed several times with alcohol and deionized water then dried at 60 °C.

Synthesis of Co_3O_4/ZnO core/shell NPs nanoparticles

To prepare Co_3O_4/ZnO core/shell NPs, 1.29 g of CoCl2 and ZnO NPs (as-synthesized) were dissolved in a mixture of 20 mL of water and 5 mL NH_4OH and then added 80 mL of ethanol drop by drop for 60 min at 60 °C with stirring for 3 hours until the sol was converted to gel. Finally, the dried gel was calcined at 300 °C for 4 h to obtain Co_3O_4/ZnO core/shell NPs.

Characterization and measurement

Co_3O_4/ZnO core/shell NPs nanoparticles were characterized by X-ray diffraction using Shimadzu 7000 Diffractometer operating with CuKα ($\lambda = 0.15406$ nm) with a scan rate of 2 min^{-1} for 2θ values between 20° and 80°.

In EDAX attaching the particles to 12.5 mm diameter Al when accelerating voltage was 20.0 kV, working distance = 10 mm, Spot size = 4.5 (EDX). In secondary electron imaging mode at different magnifications, the images were digitally recorded at a resolution setting of 1024 × 884 pixels. EDX analysis was performed using EDAX Genesis XM4 system. Standardless ZAF options were used to determine elemental contents.

The Transmission Electron Microscopy (TEM) studies were performed [High Resolution Transmission Electron Microscope (HRTEM) JEOL–JEM-1011, Japan]. The samples for TEM were prepared by making suspension from the powder in deionized water. A drop of the suspension was put into the carbon gride and left to dry. The optical properties of Co_3O_4/ZnO core/shell NPs structures were characterized by UV–Vis absorption (UV–Vis spectrophotometer Model JASCO V-670, Japan instrument). The electrical properties were measured at room temperature by Hioki (LCR Hitester 3532–50). The frequency dependence of electrical properties for prepared samples was measured from 50 Hz to 5 MHz.

Results and discussion

EDAX and XRD

The elemental contents of CZ core/shell NPs were determined using standard less ZAF option, as shown in Fig. 1. The spectra obtained during EDAX studies were used to carry out the quantitative analysis. Quantitative analysis in Fig. 1 proved high Cobalt contents (36.16%) in the examined samples. The presence of zinc, oxygen, and carbon, the contents of which amounted to 32.63, 23.59, and 7.62%, respectively, was also shown.

XRD patterns of Co_3O_4/ZnO core/shell NPs are detailed in Fig. 3. The XRD for Co_3O_4/ZnO core/shell NPs showed that the major peaks refer to ZnO hexagonal wurtzite structure in agreement with JCPDS card: 36-1451. The XRD patterns of the CZ core/shell NPs in Fig. 2 are located at (2θ) match with the reflection of (100), (002), (101), (102), (110), (103), (200), (112), and (201) crystal planes, respectively [9, 10]. Co_3O_4 peaks appear as secondary phase attributed to cubic spinel Co_3O_4 JCPDS card: 42-1467. These peaks located at (2θ) match with the reflection of (220), (311), and (400) crystal planes [11]. In XRD, the core NPs are fading due to a considerable amount of ZnO NPs in the shell [12].

TEM

TEM images are used to study the morphological aspects of the CZ NPs. Figure 3a, b presents results which confirm the formation of CZ core/shell NPs and the images show nearly spherical nanoparticles. The TEM micrograph

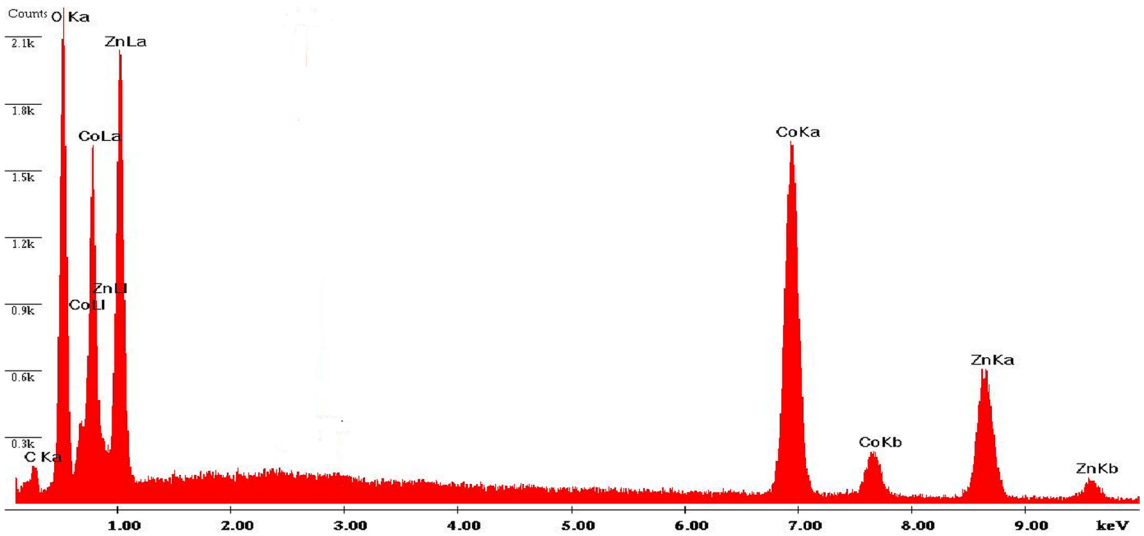

Fig. 1 EDAX images for CZ core/shell NPs

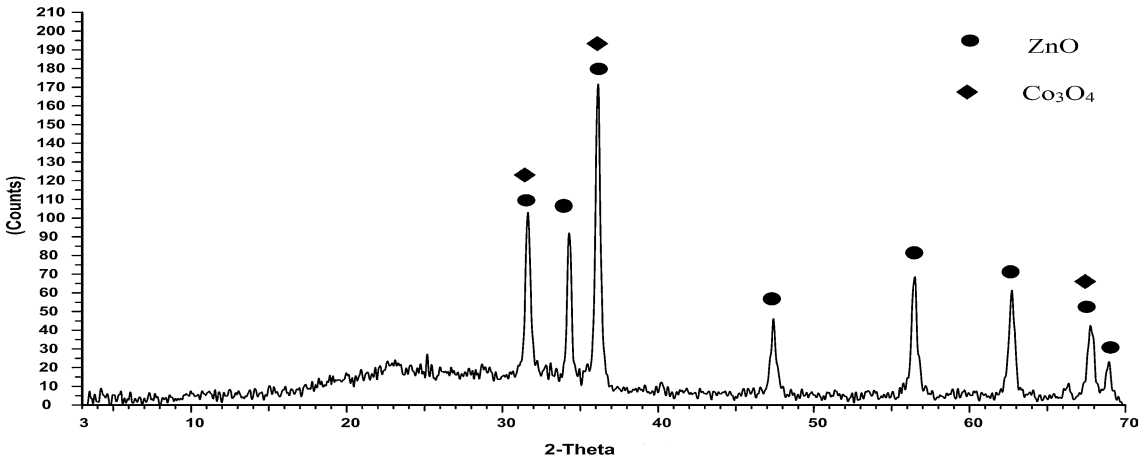

Fig. 2 XRD pattern in CZ core/shell NP

showed CZ core/shell NPs. Figure 3a, b shows that the Co_3O_4 cores appear darker than the ZnO shell. The result of TEM shows that the particles size of our sample is around 12 nm.

In TEM images, a clear interface between the core and the shell can be observed. The edge of the shell shows lower intensity than the core (Fig. 3). It can occur as a result of [13]:

1. The molar mass of the material in the shell being smaller than in the core ($Z_{Co_3O_4}$) = 240.80 g/mol, Z_{ZnO} = 81.38 g/mol.
2. The electron beam finding the smaller amount of material at the edge of NPs.

Optical properties

The optical absorption spectra of CZ core/shell NPs were obtained in the wavelength range from 200 to 800 nm using UV–Vis spectrophotometer (JASCO V-670, Japan instrument), as shown in Fig. 4a. The bulk zinc oxide (ZnO) has wide bandgap (WBG) of 3.37 eV, the semiconductors (WBG) are semiconductor materials which have a relatively large bandgap compared to conventional semiconductors [14], and the bulk Co_3O_4 has a bandgap between 2.85 and 1.70 eV [15]. The optical absorption spectrum of CZ core/shell NPs has been carried out using UV–Vis spectrophotometer. Figure 4a also shows the absorption peaks at 410 and 262 nm for CZ core/shell NPs. The first band at 410 nm

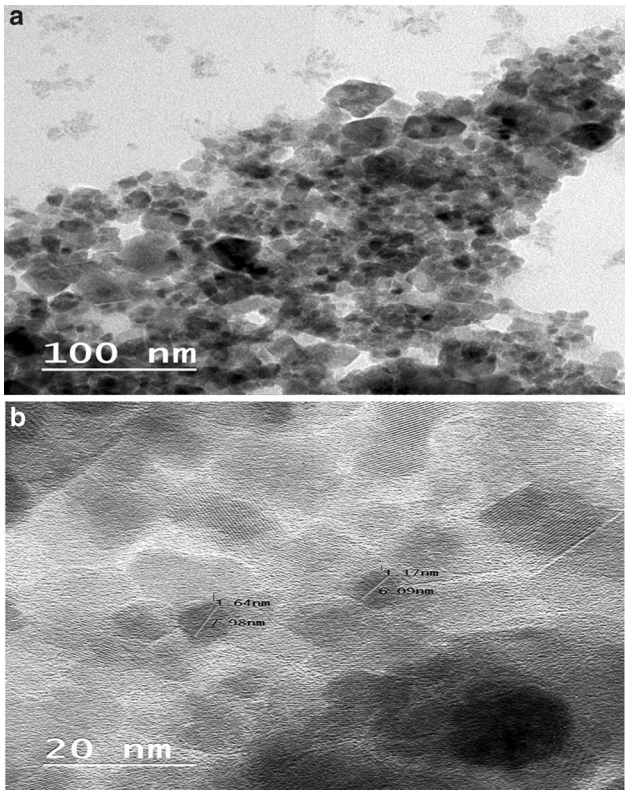

Fig. 3 **a**, **b** TEM images for CZ core/shell NPs

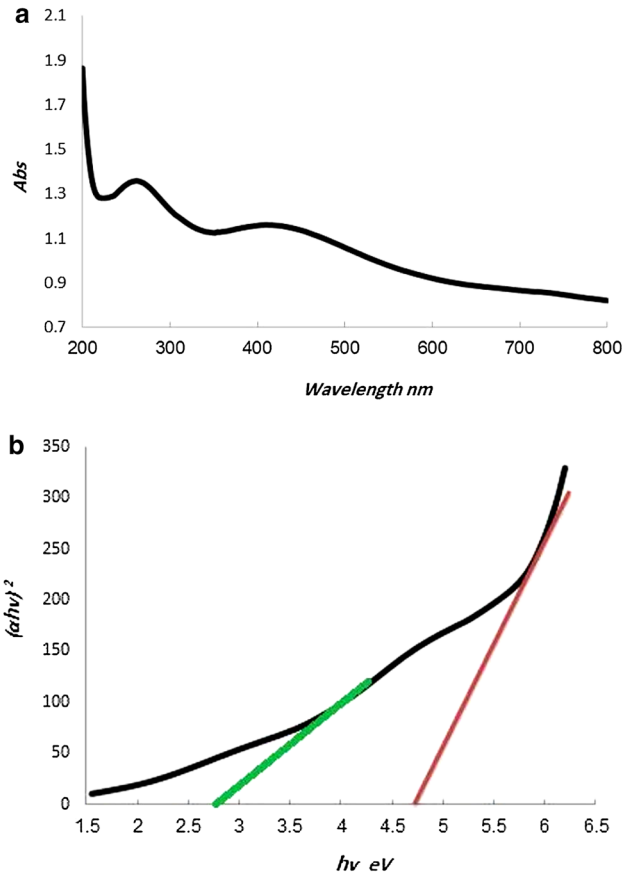

Fig. 4 Optical absorption spectra of the CZ NPs core/shell in the wavelength range from 200 to 800 nm (**a**) and plot of $(\alpha h\nu)^2$ versus $h\nu$ for the CZ NPs core/shell (**b**)

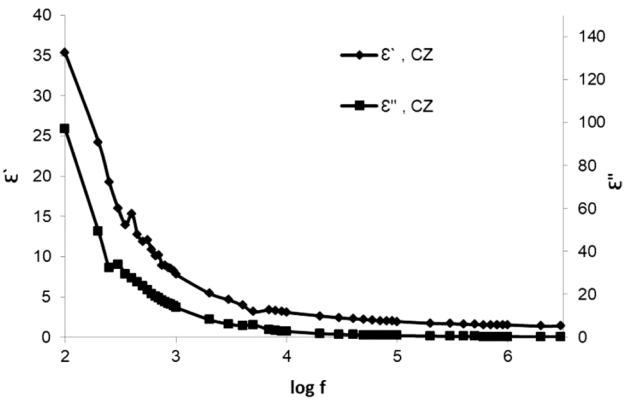

Fig. 5 Dielectric constant $\boldsymbol{\varepsilon'}$ and dielectric loss $\boldsymbol{\varepsilon''}$ as a function of frequency for CZ NPs core/shell at room temperatures

indicates change transfer or the second band appears at 262 nm; this absorption peak around 262 nm was observed. These absorption peaks in the UV region can be attributed to the local Plasmon resonance [16]. To determine the optical bandgap of the CZ core/shell NPs, we plotted $(\alpha h\nu)^2$ versus $h\nu$, where α is the absorption coefficient, and $h\nu$ is the photon energy [17]. A typical plot is shown in Fig. 4b. The bandgap of the CZ core/shell NPs was evaluated from the plot to be 4.97 eV, which showed blue shift compared to bulk ZnO and bulk Co_3O_4. The blue shift is due to a reduction in the particles size, as TEM result showed that the ZnO shells are fragile and Co_3O_4 p-type magnetic semiconductor at core next to n type of ZnO in shell influences on the properties of NPs and makes a blue shift in CZ core/shell NPs [18]. The p–n-type core–shell heterojunction can reinforce the charge separation effect under UV [19]. In addition, we observed another beak with gap energy 2.75 eV.

Dielectric properties

Dielectric constant (ε') and dielectric loss (ε'') frequency of CZ core/shell NPs as a function of frequency range (50 Hz–5 MHz) at room temperature are shown in Fig. 5. The spectrum for CZ core/shell NPs sample show that dielectric constant (ε') decreases exponentially with the increase of frequency. The dielectric constant (ε') proximate a constant value at high frequencies due to the shortage of dipoles to twirl quickly leading to a delay between applied field and frequency of wobbling dipole [20]. The

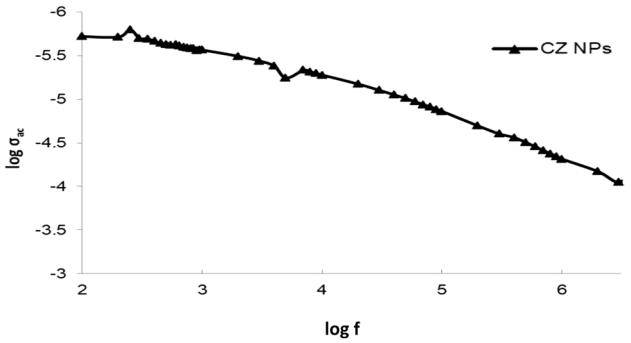

Fig. 6 log σ_{ac} as a function of frequency for CZ core/shell NPs at room temperatures

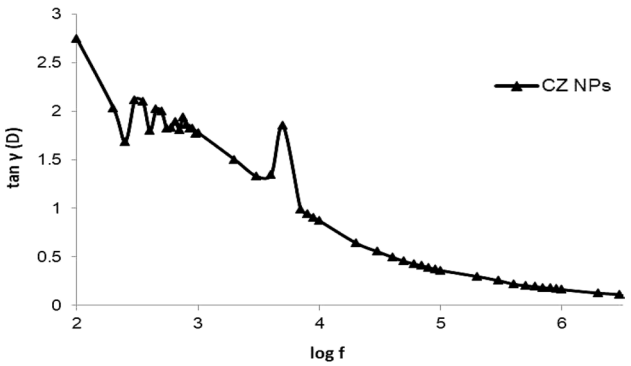

Fig. 7 Dielectric loss tangent *D* as a function of frequency *log f* for CZ core/shell NPs at room temperatures

high values of ε' at low frequencies may be attributed to the interfacial polarization which is appearing in materials composed of different phases [21]. In addition, in Fig. 5, it is clearly shown that dielectric loss (ε'') at room temperatures decreases with the frequency of CZ core/shell NPs.

The frequency dependence of ε'' in Fig. 5 can be interpreted, by the following equation approbating to the free electron theory: $\varepsilon'' = \delta/2\ \pi\ \varepsilon^0 f$, where f is frequency, δ is the electrical conductivity, and $\varepsilon 0$ is the dielectric constant in a vacuum. Figure 6 shows the relationship between conductivity and frequency. The conductivity of CZ core/shell NPs generates from its free electrons. In addition, ε'' is critical to the absorbing frequency which becomes a defiance for technological applications [22]. σac presents a flat frequency plateau at lower frequencies as is shown in Fig. 6. However, the conductivity, as a frequency-dependent behavior, shows itself at higher frequencies. It may be due to hopping-type conduction at a high-frequency range [23].

The decrease in particles size to nanometric scale has been found to produce massive reduction in the tan δ (D) value, as shown in Fig. 7. The value of tan δ depends on many factors such as synthesis methods and sample composition.

ε', ε'', and tan of CZ core/shell NPs exhibit the electrical energy storage capacity and average loss in the materials [24]. The dielectric constant (ε') and the tan δ values of investigated CZ core/shell NPs at 1 kHz are 7.8 and 1.77, respectively. It was also observed that the dielectric constant (ε') of CZ core/shell NPs at 1 kHz under room temperature is less than the values of ZnO (40 nm) [25] and higher than ε' value of Co_3O_4 (36 nm) [26] that measured in the previous studies where the ε' value were about 40 and 7 for ZnO and Co_3O_4 at 1 kHz under room temperature, respectively.

Conclusion

CZ core/shell NPs with nearly spherical nanoparticles have been synthesized successfully by the sol–gel method. The particles size CZ core/shell was around 12 nm. The optical properties study by UV–Vis spectroscopy to estimate the bandgap of core/shell NPs, and band-gap value of CZ core/shell NPs is higher than bandgap of bulk ZnO and Co_3O_4. The dielectric measurements indicate that the dielectric constant of CZ core/shell NPs decreases, in the high-frequency range.

Acknowledgements The author would like to show her gratitude towards Professor Magdah Dawy of the National Research Center in Cairo, Egypt, whose expertise greatly assisted the research.

References

1. Wu, B., Zheng, N.: Surface and interface control of noble metal nanocrystals for catalytic and electrocatalytic applications. Nano Today **8**, 168–197 (2013)
2. Chaudhuri, R.G., Paria, S.: Core/shell nanoparticles: classes, properties, synthesis mechanisms, characterization, and applications. Chem. Rev. **112**, 2373–2433 (2012)
3. Kalele, S., Gosavi, S.W., Urban, J., Kulkarni, S.K.: Nanoshell particles: synthesis, properties and applications. Curr. Sci. **91**, 1038–1052 (2006)
4. Goncharenko, A.V.: Optical properties of core-shell particle composites. I. linear response. Chem. Phys. Lett. **286**, 25–31 (2004)
5. Zhao, W., Gu, J., Zhang, L., Chen, H., Shi, J.: Fabrication of uniform magnetic nanocomposite spheres with a magnetic core/mesoporous silica shell structure. J. Am. Chem. Soc. **127**, 8916–8917 (2005)
6. Yin, J.S., Wang, Z.L.: In-situ structural evolution of self-assembled oxide nanocrystals. J. Phys. Chem. **101**, 8979–8983 (1997)
7. Rouhi, J., Mahmud, S., Naderi, N., Raymond, C., Mahmood, M.: Physical properties of fish gelatin-based bio-nanocomposite films

incorporated with ZnO nanorods. Nano Res. Lett. **8**, 364–370 (2013)
8. Nidhi, S., Karan, B., Dipak, V., Shashank, T.M.: Ultrasound and conventional synthesis of Ceo_2/Zno nanocomposites and their application in the photocatalytic degradation of rhodamine B dye. J Adv Nanomater. **2–3**, 133–145 (2017)
9. Talaat, M.H., Jamil, K.S., Harrison, R.G.: Structure, optical properties and synthesis of Co-doped ZnO superstructures. Appl. Nanosci. **3**, 133–139 (2013)
10. Hyun, T.J., Eui, M.J., Sang, H.P., Pushparaj, H.: Synthesis and characterization of CoO–ZnO catalyst system for selective Co oxidation. Int. J. Control Autom. **8**, 31–40 (2013)
11. Hui, X., Junxia, Z., Yong, C., Junxia, W., Junlong, Z.: Preparation and performance of Co_3O_4–NiO composite electrode material for supercapacitors. RSC Adv. **4**, 15511–15517 (2014)
12. Gillet, J.N., Meunier, M.: General equation for size nano characterization of the core-shell nanoparticles by X-ray photoelectron spectroscopy. J. Phys. Chem. B **109**, 8733–8740 (2005)
13. Singh, S., Khare, N.: Self assembled CdS/ZnO core/shell nanorods heterostructure: an efficient and stable photocatalyst. J. Nanosci. Nanotechnol. **16**, 7404–7410 (2016)
14. Barakat, N.A.M., Khil, M.S., Sheikh, F.A., Kim, H.Y.: Synthesis and optical properties of two cobalt oxides (CoO and Co_3O_4) nanofibers produced by electrospinning process. J. Phys. Chem. C **112**, 12225–12233 (2008)
15. Sarfraz, A.K., Hasanian, S.K.: Size dependence of magnetic and optical properties of Co_3O_4 nanoparticles. Acta Phys. Pol. Ser. A. **125**, 139–144 (2014)
16. Xianfeng, Z., Guofang, S., Yu, L., Hanning, D., Xiaoyu, Y., Shaozhuan, H., Hongen, W., Chao, W., Zhao, D., Bao-Lian, S.: Self-templated synthesis of microporous CoO nanoparticles with highly enhanced performance for both photocatalysis and lithium-ion batteries. J. Mater. Chem. **1**, 1394–1400 (2013)
17. Mallick, P., Dash, B.N.: X-ray diffraction and UV-visible characterizations of α-Fe_2O_3 nanoparticles annealed at different temperature. Nanosci. Nanotechnol. **3**, 130–134 (2013)
18. Nada, J., Sapra, S., Sarma, D.D.: Size-selected zinc sulfide nanocrystallites: synthesis, structure, and optical studies. Chem. Mater. **12**, 1018–1024 (2000)
19. Yuanyuan, Z., Peifei, T., Dong, M., Bing, L., Qinzhuang, L., San, C., Yongxing, Z.: A facile route to the preparation of highly uniform ZnO@TiO_2 core-shell nanorod arrays with enhanced photocatalytic properties. J. Chem. **2107**, 8 (2017)
20. El Sayed, A.M., El-Gamal, S.: Synthesis and investigation of the electrical and dielectric properties of Co_3O_4/(CMC + PVA) nanocom- posite films. J Polm. Res. **22**, 97–108 (2015)
21. Tataroğlu, B., Altındal, S., Tataroğlu, A.: The C–V–f and G/ω–V–f characteristics of Al/SiO_2/p-Si (MIS) structures. Microelectron. Eng. **83**, 2021–2026 (2006)
22. Chao, F., Nannan, B., Xianguo, L., Chuangui, J., Kai, H., Feng, X., Yuping, S., Siu, W.O.: Synthesis, characterization and microwave dielectric properties of flower-like $Co(OH)_2$/C nanocomposites. Mater. Res. **17**, 920–925 (2014)
23. Chisca, S., Musteata, V.E., Sava, I., Bruma, M.: Dielectric behavior of some aromatic polyimide films. Eur. Polym. J. **47**, 1186–1197 (2011)
24. Choudhary, S.: Dielectric and electrical properties of different inorganic nanoparticles dispersed phase separated polymeric nanocomposite bilayer films. Indian J. Chem. Technol. **24**(3), 311–318 (2017)
25. Amrut, S.L., Satish, J.S., Raghumani, S.N., Ramchandra, B.P.: Low temperature dielectric studies of zinc oxide (ZnO) nanoparticles prepared by precipitation method. Adv. Powder Technol. **24**, 331–335 (2013)
26. Durai, M.P.D., Sadaiyandi, K., Mahendran, M., Suresh, S.: Precipitation method and characterization of cobalt oxide nanoparticles. **123**, 264 (2017). https://doi.org/10.1007/s00339-017-0786-8